

PRESSURE MODE FLUID DYNAMIC GAUGING UNDER EXTREME CONDITIONS

A. Ali^{1,*}, Y.M.J. Chew², P. Gordon¹, B. Salley¹, W.R. Paterson¹ and D.I. Wilson¹

¹ Department of Chemical Engineering & Biotechnology, New Museums Site, Pembroke Street, Cambridge CB2 3RA, UK

*E-mail (aa620@cam.ac.uk):

² Department of Chemical Engineering, University of Bath, Claverton Down, Bath BA2 7AY, UK

ABSTRACT

We report proof-of-concept results for pressure mode fluid dynamic gauging (FDG) for measuring the thickness and strength of soft solid fouling layers immersed in an opaque liquid *in situ* and in real time. Two applications of this mode are presented here. The first, termed *high pressure FDG*, makes measurements on the inner rod of an annular test section at elevated temperatures and pressures. The second, termed *low stress FDG*, is designed to measure the thickness of biofilms immersed in aqueous solutions while subjecting the layer to low shear stresses. Data are presented for high pressure FDG from tests using mineral oil at temperatures and pressures up to 140 °C and 10 bara, respectively. The practical working range of the gauge, *i.e.* $0.05 < h/d_t < 0.25$, proved to be unaffected by the pressure and temperature [where h dimensionless clearance and d_t is the nozzle throat diameter, which varies from 1 – 2 mm]. At smaller h/d_t values the pressure drop across the nozzle is very high and this can serve as an alarm for close approach. A lower limit for gauging flow rates is identified from the response at low Reynolds numbers. A configuration was identified for low stress FDG which achieved a compromise between thickness measurement accuracy and shear stress imposed on the layer. This was used to monitor the thickness of cyanobacterial biofilms on three different substrates over a four week period. Similar growth rates were observed but biofilms grown on indium tin oxide and 304 stainless steel exhibited cohesive failure, whilst those on glass exhibited adhesive breakdown.

INTRODUCTION

The build-up of fouling deposits on heat transfer surfaces is a serious industrial problem affecting heat exchanger performance and operability. The extent of fouling is often quantified experimentally through the reduction in heat transfer performance or increase in pressure drop across units. Understanding the mechanisms involved in fouling and cleaning requires careful experimentation to measure the deposit strength and thickness as well as other parameters.

Fouling layers can be formed from flowing liquids and gases. Since many fouling layers formed from liquids are soft and deform readily when removed from their native

liquid environment, and the liquids are usually opaque, measuring their thickness reliably under experimental conditions is challenging. Fluid dynamic gauging (FDG) is a non-contact measurement technique developed by Tuladhar *et al.* (2000) to measure the thickness of soft fouling layers in liquid environments *in situ* and in real time.

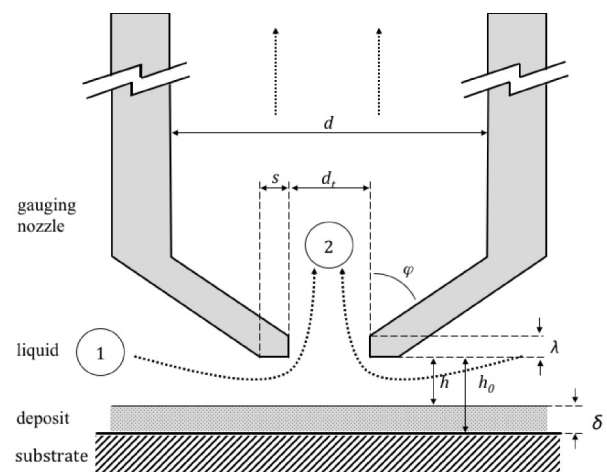


Figure 1. Schematic of an FDG gauging nozzle (not to scale). Dotted lines denote liquid flow path. Stations (1) and (2) indicate the region over which the majority of the pressure drop across the nozzle is generated. Symbols: δ – thickness of deposit layer; d_t – inner diameter of nozzle; s – lip width; ϕ – nozzle angle; d – inner tube diameter.

The principle of FDG is illustrated in Figure 1. A nozzle is located at a distance, h_0 , from a solid surface immersed in liquid. h , is very sensitive to both the liquid mass flow rate through the nozzle, \dot{m} , and the pressure drop across the nozzle, ΔP_{12} . Measurements of \dot{m} and ΔP_{12} allow h to be calculated without making contact with the layer. The range of clearances over which useful measurements can be made is $h/d_t < 0.25$, where d_t is the inner diameter of the gauging nozzle. The thickness of the fouling layer, δ , can then be calculated by difference, viz.

$$\delta = h_0 - h \quad (1)$$

where h_0 is measured independently or when the substrate is clean.

The primary requirement for the technique is that the surface being gauged remains stiff over the duration of the test. The flow of liquid underneath the nozzle at low values of h can generate significant shear stresses on the deposit. Chew *et al.* (2004a,b) demonstrated how this can be exploited to determine the strength (or yield point) of a deposit layer. They quantified the normal and shear stresses imposed on the surface using computational fluid dynamics (CFD) simulations for flows in the laminar and inertial regime and demonstrated that the shear stresses generated in the nozzle region were dominated by the gauging flow contribution, with little influence from the bulk. It should be noted that the flow through the nozzle and past station 2 in Figure 1 is set to lie in the laminar regime.

Tuladhar *et al.* (2000) demonstrated the FDG concept with measurements on flat surfaces immersed in a stagnant bath of liquid. The technique has since been shown to work well in applications where the bulk liquid is flowing, including ducts of square (Tuladhar *et al.*, 2003) and annular (Gu *et al.*, 2011a, b) cross-section.

Many of the FDG applications reported to date have involved liquids at temperatures near ambient (10 – 110 °C) and pressures ranging from 1–3 bara. Industrial applications often feature higher temperature and pressure conditions. A particularly important area is the fouling of heat exchangers used to process crude oil, where the liquid can reach 300 °C and 30 bara. Macchietto *et al.* (2010) reported the development of an experimental fouling test rig designed to operate under these conditions. One of the test sections on their high temperature and pressure oil (HIPOR) fouling unit employed an annular flow section with a heated central rod. This paper reports the performance of an FDG device for measuring deposit layer thickness in apparatuses such as the HIPOR unit where, in addition to the high temperature and pressures, the liquid is opaque and flammable. This is the *high pressure* extreme: in these tests the flow rate of gauging liquid must be small, both to avoid disturbing the flow pattern in the apparatus and to ensure safe operation.

The second extreme is where the fouling layers are weak and readily deformable, such as biofilms, requiring the shear stress exerted by the gauging flow must be carefully controlled. Mohle *et al.* (2007) demonstrated that FDG could be used to study biofilms, but higher resolution would require an improved method. This is the *low stress* extreme. This paper reports recent work which has allowed both extremes to be studied, based on similar principles but quite different hardware.

2. Pressure Mode Gauging

In addition to h and ΔP_{12} , the mass flow rate is sensitive to the nozzle throat diameter, d_t , the nozzle shape, the liquid density, ρ , and viscosity, μ . The dimensional analysis presented by Tuladhar *et al.* (2000) showed that ΔP_{12} is determined by one flow and two geometric parameters, *viz.*

$$C_d = f \left\{ \frac{h}{d_t}, \frac{s}{d_t}, Re_t \right\} \quad (2)$$

where C_d is the discharge coefficient, which is the ratio of \dot{m} to the ideal mass flow rate through the nozzle and accounts for the energy losses associated with flow around the nozzle:

$$C_d = \frac{\text{actual mass flow rate}}{\text{ideal mass flow rate}} \\ = \frac{\dot{m}}{\frac{\pi}{4} d_t^2 \sqrt{2\rho\Delta P_{12}}} \quad (3)$$

Re_t is the Reynolds number evaluated at the throat of the nozzle diameter.

FDG devices initially employed ‘mass-mode’ operation, whereby ΔP_{12} is held constant and \dot{m} measured to give h/d_t . Equations (2) and (3) show that \dot{m} is then uniquely related to h/d_t for a given nozzle shape. Mass-mode operation is ideally suited to operation at near-ambient pressure, as a hydrostatic head can supply a stable pressure driving force cheaply. Controlling pressure differences to small values (typically a few kPa for a 1 mm nozzle) at higher pressures is challenging, and the associated variation in flow rate of a hazardous liquid (and the risk of spillage if pressure control is lost) means that mass-mode operation is then unattractive for high pressure FDG. A second reason is that under certain conditions, duct flow FDG can exhibit several steady states in C_d at a given h/d_t (Tuladhar *et al.*, 2003). This occurs when \dot{m} is a significant fraction of the bulk flow rate, leading to strong interaction between the bulk and gauging flows. In practice, the amount of liquid to be withdrawn through the gauging nozzle will be set to be a small fraction of the total flow rate in order to avoid significant changes in the bulk flow pattern.

Low stress FDG requires small pressure drops. Whilst it is possible to maintain a small hydrostatic head to drive a flow, the pressure losses across ancillary piping, instruments and connections must be minimised and this can be problematic.

Considerations such as these prompted the development of ‘pressure-mode’ FDG. Here, \dot{m} is set and ΔP_{12} is measured as h/d_t is varied. Inspection of equations (2) and (3) shows that C_d is proportional to $\Delta P_{12}^{-0.5}$: ΔP_{12} increases as the nozzle approaches the surface and this confers advantages in terms of the accuracy required for a differential pressure transducer as well as setting alarms to warn of close approach to the surface. Pressure-mode duct flow FDG has been demonstrated in cross-flow microfiltration (Lister *et al.* 2010; Lewis *et al.*, 2012), ultra-filtration (Jones *et al.*, 2012) and annular duct flow (Gu *et al.*, 2009; 2011a). Pressure-mode FDG is easier to implement at higher pressures and overcomes the problem of multiple steady states, as \dot{m} can be restricted to a small fraction of the bulk flow.

In addition, particularly for low stress FDG, the shear stress imposed on the surface, τ , is directly proportional to \dot{m} , and is therefore relatively easy to control. The highest shear stresses are found underneath the nozzle inner rim and a reliable estimate of the largest τ values is given by the result for flow between parallel discs (Middleman, 1998):

$$\tau_{max} = \frac{6\mu}{\pi\rho d_t} \frac{\dot{m}}{h^2} \quad (4)$$

In contrast, it is difficult to control τ directly in mass mode measurements.

The use of pressure mode gauging for high pressure and low stress FDG, employing very different apparatuses is described in turn.

3 High Pressure FDG

3.1 FDG probe

The nozzle system was designed to make measurements on the surface of the inner rod of the HIPOR annular fouling test rig described by Macchietto *et al.* (2010). The annulus dimensions were inner rod diameter, 24 mm, and internal diameter of the outer pipe, 35 mm. The nozzle design is similar to that reported by Gu *et al.* (2009), namely $d_t = 1$ mm, $s = 0.5$ mm, with an internal nozzle angle, ϕ , of 45°. The gauging tube internal diameter, d , was 4 mm with a wall thickness of 2 mm. The device was fabricated from 316L stainless steel and all connections were fabricated using 316L stainless steel (SS) ¼ inch Swagelok® tubing. A detailed description of the nozzle mounting and peripherals is given in Ali *et al.* (2013). The position of the nozzle is manipulated by a stepper motor which can withdraw the nozzle into a housing in the outer annulus wall when measurements are not being made.

Pairs of reinforced PTFE seals provided liquid isolation. Liquid passed through the nozzle, along the gauging tube and then through a series of holes in the tube wall, sized to give a low pressure drop, into a precision piston flow meter (Max Machinery, model 214-410). The position of the nozzle was recorded using a displacement sensor. The absolute system pressure was recorded using a pressure gauge while the pressure drop across the FDG probe was measured using a differential pressure transducer (SensorsONE, PD-33X) connected to tapings on the annulus and the probe exit, located at the same elevation.

For the tests reported here, the probe was mounted on a short (approximately 30 cm long) section of annular test section. A mineral oil (Paratherm™ NF, density 887 kg/m³ and viscosity 44 mPa s at ambient temperature and pressure; Paratherm™ Corporation, 2011) was pumped from a reservoir around the system using a gear pump (Ismatec Instruments, MVZ-01412-3A) controlled via the pump speed and a manual control valve. The absolute pressure was set independently by pressurizing the oil reservoir using nitrogen gas. Data from the flow meter, thermocouple, displacement sensor and differential pressure transducer were collected on a PC (Athlon XP 2200+, 1 GB RAM) running LabView™ version 8.0. This application was also used to control the stepper motor.

The temperature of the test apparatus was adjusted using electrical heating tape wrapped around the test section, piping, and reservoir. Thermocouples located in the annulus and piping downstream of the FDG probe recorded the temperature. The maximum temperature which could be achieved safely using this arrangement was 140°C. Slow leaks were observed at pressures around 10 bara so higher pressures were not studied in these tests.

3.2 Testing protocol

Calibration curves (plots of C_d versus h/d_t) were obtained by starting from some distance away (*i.e.* $h/d_t > 1$), then moving the gauging nozzle towards the inner rod surface in steps, recording ΔP_{12} , \dot{m} and h at each step. The process was then reversed and measurements made as the nozzle retreated from the surface. Advancing and receding data sets showed good reproducibility (the data sets overlapped) and the precision of h/d_t was < 5 μm . Individual data points took approximately 30 s to record: the speed of experiments was chiefly determined by the time taken for the system to come to thermal steady state. When measuring deposit layer thickness, the device could be programmed to maintain a constant nozzle-surface separation, as reported by Gordon *et al.* (2010), to ensure that the shear forces exerted by the gauging flow on the fouling layer remain constant.

3.3 CFD Simulations

A short set of simulations of the high pressure FDG device operating in quasi-static flow (*i.e.* no duct flow: only gauging flow) was performed and are presented alongside selected experimental results to demonstrate that the calculations are tractable on a standard PC.

As the liquid is Newtonian, approximately isothermal and incompressible, the steady-state Navier-Stokes and continuity equations describe the fluid dynamics:

$$\text{Continuity:} \quad \nabla \cdot \mathbf{v} = 0 \quad (5)$$

$$\text{Navier Stokes} \quad \rho \mathbf{v} \cdot \nabla \mathbf{v} = -\nabla P + \mu \nabla^2 \mathbf{v} + \rho \mathbf{g} \quad (6)$$

where \mathbf{v} is the velocity vector and P is the pressure. The acceleration due to gravity, \mathbf{g} , is set to zero as its contribution is small (see Chew *et al.*, 2004b). The simulations were performed using the finite element modelling package, COMSOL Multiphysics® version 4.3, employing the SPOOLES direct solver running on a PC (2.61 GHz dual core processor and 3.25 GB RAM). The domain was modelled with tetrahedral elements. The largest velocity and pressure gradients were located in the region below the nozzle, so mesh elements were concentrated there. Solution times varied from 5 to 20 minutes to compute. The boundary conditions, mesh refinement and solution criteria are reported in Ali *et al.*, (2013).

3.4 Ambient pressure and temperature FDG

The plot of ΔP_{12} against h/d_t for fixed \dot{m} at ambient conditions in Figure 2 shows that the device performs pressure-mode gauging successfully. The behaviour expected from tests conducted with water in Perspex devices by Gu *et al.* (2009) is evident: distant from the

surface ($h/d_t > 0.25$) the pressure drop across the nozzle shows little effect of clearance, whereas for $h/d_t < 0.25$, ΔP_{12} increases noticeably with clearance.

The corresponding C_d values are plotted alongside the raw data. The C_d values have greater error bars as these values require the measurement of \dot{m} , which itself has an associated error. The $C_d - h/d_t$ profile, termed a calibration plot, shows three regions. In region A, $h/d_t < 0.05$, C_d is almost constant (here, ~ 0.05) and less sensitive to clearance. On flat substrates, C_d approaches zero as $h/d_t \rightarrow 0$ and the lower limit observed here arises from the curvature of the surface. Region A was labelled the ‘curvature region’ by Gu *et al.* (2009). It serves a useful purpose in these applications as ΔP_{12} increases strongly as the nozzle approaches the surface and can be used to trigger an alarm for close approach. In region B, $0.05 \leq h/d_t < 0.25$, C_d increases monotonically with h/d_t and is the region in which FDG thickness measurements can usefully be made.

In Region C, $h/d_t > 0.25$, C_d is relatively insensitive to h/d_t , and approaches a limiting value, labelled C_d^∞ , asymptotically. In gauging measurements the nozzle will normally start distant from the surface and ΔP_{12} will therefore not change until it approaches the surface. At higher P , where equipment failure (*e.g.* leakage) is more likely to occur, comparing C_d in region for $h/d_t > 0.25$ can be used to check whether the nozzle is blocked or other parts are functioning correctly. Blockage can also be avoided by selecting a nozzle diameter several times larger than the characteristic length of foulant species.

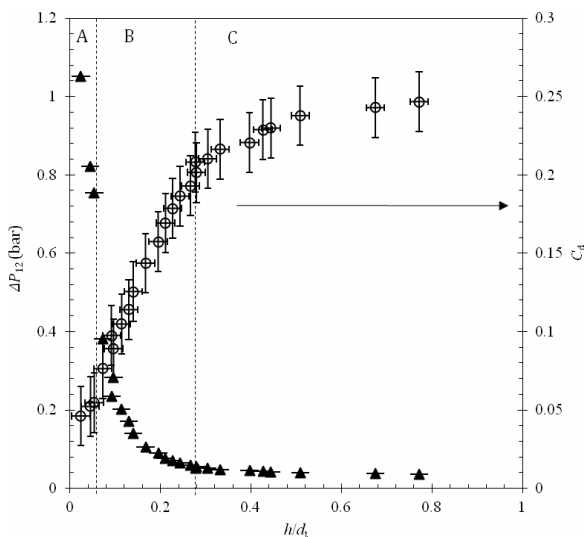


Figure 2. Effect of clearance on pressure drop across nozzle and the calculated discharge coefficient. Conditions: $P = 1$ bara, $T = 19$ °C, $\dot{m} = 0.5$ g/s, $Re_t \sim 15$. Vertical dashed lines separate the regions A, B and C. Solid symbols – ΔP_{12} ; open symbols – C_d .

The C_d^∞ value in Figure 2 is noticeably smaller than the range of values reported by Gu *et al.* (2011a,b), of $0.5 < C_d^\infty < 0.9$. Similarly low values of C_d^∞ were reported for

experimental and CFD simulation studies of FDG on flat surfaces at low Re_t by Chew *et al.* (2004b). This is a feature of the relatively slow flow: as Re_t approaches unity, viscous losses in the flow become comparable to inertial losses and the Bernoulli equation (which underpins the definition of C_d in Equation (3)) does not provide an appropriate estimate of the ideal fluid flow. Chew *et al.* (2004a)’s CFD simulations, supported by experiments using viscous liquids, showed that C_d becomes strongly dependent on Re_t and independent of h/d_t for $Re_t < 8$. In the creeping flow regime C_d becomes proportional to $Re_t^{0.5}$.

The $C_d - h/d_t$ profiles in Figure 3 show a marked difference in behaviour between $Re_t = 1.1$ and $Re_t = 7$, which was achieved by increasing the flow rate (at constant temperature). The C_d^∞ value increases with Re_t , as reported by Chew *et al.* (2004a) for FDG on flat surfaces. These results indicate that there is a practical lower limit for the flow rate to be used for FDG measurements, corresponding to $Re_t \sim 10$. FDG measurements remain feasible at lower flow rates, but more accurate measuring devices are required than those used here.

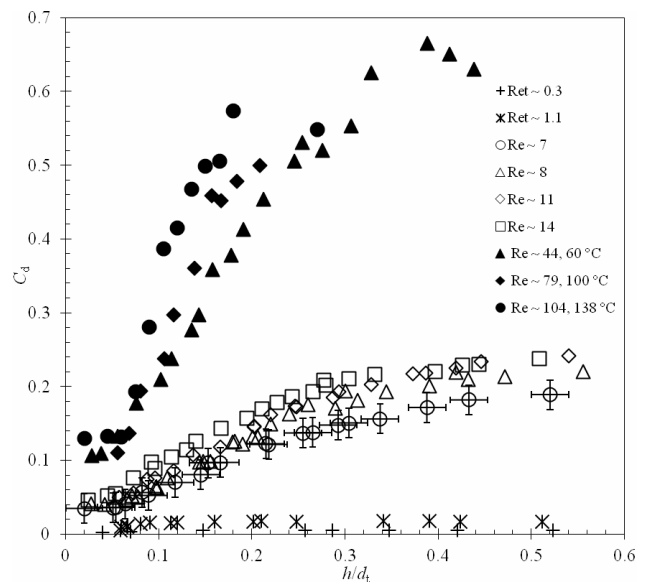


Figure 3. Effect of gauging flow rate on calibration plot profiles. Conditions: 1 bara. Error bars marked on $Re_t \sim 7$ data set. Open symbols – 19 °C; Solid symbols - elevated temperature, given in legend.

3.5 Higher temperature and pressure operation

Increasing the liquid temperature raises the Reynolds number via the reduction in viscosity and this has a noticeable effect on the calibration plots in Figure 3. The C_d profiles in Figure 3 show similar behaviour for 60 – 138 °C. Fewer data points were collected at the highest temperature owing to difficulties in temperature control in this test. The same mass flow rate was used in each case, namely 0.40 g/s. The similarity in profiles is consistent with the flows no longer being in the creeping regime: at these temperatures Re_t varied from 44 – 104. The C_d^∞ values of 0.6 - 0.7 are similar to those reported by Gu *et al.* (2009). A large

difference in C_d values with h/d_t is desirable for gauging, as the associated change in pressure drop across the nozzle is larger. These results suggest that a criterion for selecting the minimum flow rate is that $Re_t > 20$.

Figure 4 shows calibration plots obtained for operation at 138 °C and pressures of 1 and 10 bara. The incremental zone (region B) useful for measuring deposit thickness is evident in both tests for $0.1 < h/d_t < 0.25$. There were noticeable leaks in the higher pressure test, which have greatest impact at higher values of h/d_t (when the pressure drop across the nozzle is lowest). It should be noted that the seals used in these tests were two years old and had not been replaced since the device was first assembled. Leaks notwithstanding, these results constitute proof-of-concept evidence that pressure mode FDG is suitable for high pressure FDG operation. Some aspects of the hardware require attention in order for the device to operate reliably at elevated pressure and temperature.

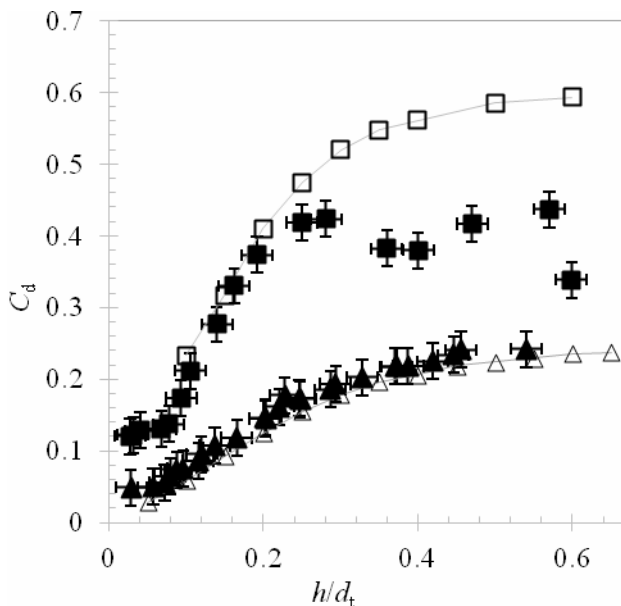


Figure 4. Comparison of experimental C_d profile with values generated by CFD simulation. Squares represent data at $P = 10$ bara, 138 °C, $Re_t \sim 205$; triangles at $P = 1$ bara, $T = 21$ °C, $Re_t \sim 11$. Solid symbols - experimental data; open symbols and dashed interpolation line - simulation results.

3.6 Comparison with CFD simulations

Figure 4 compares the experimental data with the $C_d - h/d_t$ profiles generated by the CFD simulations. The inputs to the simulation are the experimental mass flow rate and h/d_t value: ΔP_{12} is extracted from the solution and C_d calculated. The agreement is very good at ambient pressure and lies within the estimates of experimental uncertainty. Similarly good agreement was obtained at other Re_t values (data not reported). The agreement with the experimental data set at 10 bara is good for $h/d_t < 0.20$, but there is a noticeable difference between the measured C_d values and the simulations at larger values of h/d_t . This difference arises from the measured pressure drop being associated

with an uncertain mass flow rate owing to the slow leaks mentioned above.

CFD data are not reported for small clearances ($h/d_t < 0.05$) in Figure 4 as a very fine mesh was required for these cases. With greater computing resources, the curvature region could be identified directly. Moreover, this region is one in which it is not desirable to operate the gauge as C_d is not usefully sensitive to h/d_t and the shear stress imposed on the surface is at its greatest.

Flow velocity distributions generated by the CFD simulations show that at higher $Re_t (> 40)$, there is asymmetry near the nozzle and a flow recirculation regime is observed inside the nozzle throat. This may explain the difference in $C_d - h/d_t$ profiles at high $Re_t (> 40)$ and low $Re_t (< 20)$ in Figure 3. At the higher Re_t values, the presence of recirculation regions will lead to an increase in ΔP_{12} and thus larger C_d values.

The CFD simulations also yield distributions of the shear stress imposed on the inner cylinder surface during gauging tests. These are presented elsewhere (Ali *et al.*, 2013) and exhibit the features reported by Gu *et al.* (2009).

4. LOW SHEAR STRESS FDG

Biofilms are fragile and it therefore important to subject such layers to known, small shear stresses during measurement. The calibration plots for pressure mode FDG above (*e.g.* Figure 3) indicate that thickness measurements require the clearance, h , to be less than $h/d_t < 0.25$. Equation (4), in turn, can be rewritten as

$$\tau_{max} = \frac{6\mu}{\pi\rho} \frac{1}{d_t^3} \frac{\dot{m}}{(h/d_t)^2} \quad (7)$$

which emphasizes that for a given nozzle diameter, the shear stress imposed on the surface being gauged is proportional to the flow rate and $(h/d_t)^{-2}$. There is therefore a compromise to be reached between the stress imposed on the layer and the pressure drop required for reliable measurement, which can be manipulated by the flow rate and nozzle size. There are also practical limitations on nozzle size: a large nozzle will be unwieldy while a small nozzle should be larger than the characteristic length scale of the organisms or structures in the biofilm. A 2 mm diameter nozzle was selected as a suitable compromise.

Figure 5 shows how the shear stress imposed on the surface and the accuracy in measuring h with such a nozzle are expected to vary for different flow rates. The estimated uncertainty in h is based on a differential pressure transducer accuracy of ± 3 Pa. The flow rate range of 0.3–1.0 g/s is readily attained with a syringe pump. The lower limit of $h/d_t = 0.06$ was selected on the basis of strongly increasing shear stress, such that a small error in locating the nozzle could readily cause disruption. The upper limit marks the end of the incremental zone within which thicknesses can be measured reliably. The trade-off that arises between accuracy and avoiding disruption is evident.

Figure 5 indicates that larger flow rates exert higher shear stresses but yield better accuracy, so the measurement

protocol adopted used a low value of \dot{m} initially. When the presence of the biofilm was detected, at high h/d_t , \dot{m} was increased, without moving the nozzle, in order to improve the accuracy in estimating h . The nozzle could be moved towards the layer in order to improve the accuracy of the thickness measurement or to test the strength of the layer.

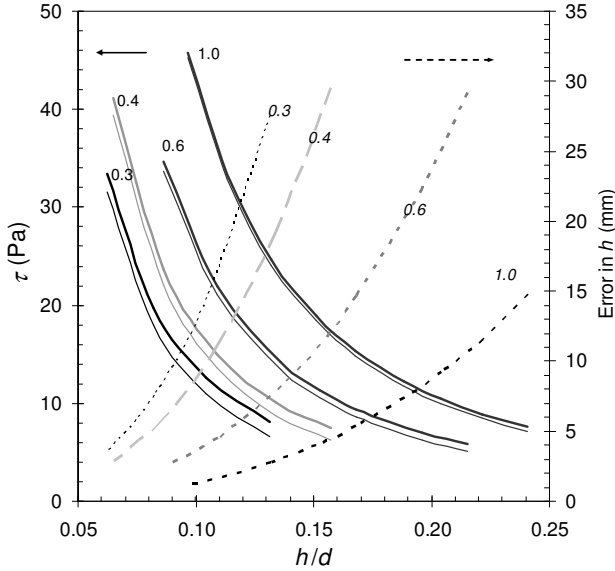


Figure 5 Effect of flow rate on (left abscissa) the shear stress imposed on the surface being gauged and (right abscissa) error in thickness measurement for 2 mm nozzle at different dimensionless clearances. Flow rate values in g/s. Gauging liquid: water at 20°C.

Figure 6 illustrates this method of measurement: the initial measurement was subject to a large uncertainty in h which decreased as the flow rate (and shear stress) increased. There is large scatter in the data due to the non-uniformity of the biofilm.

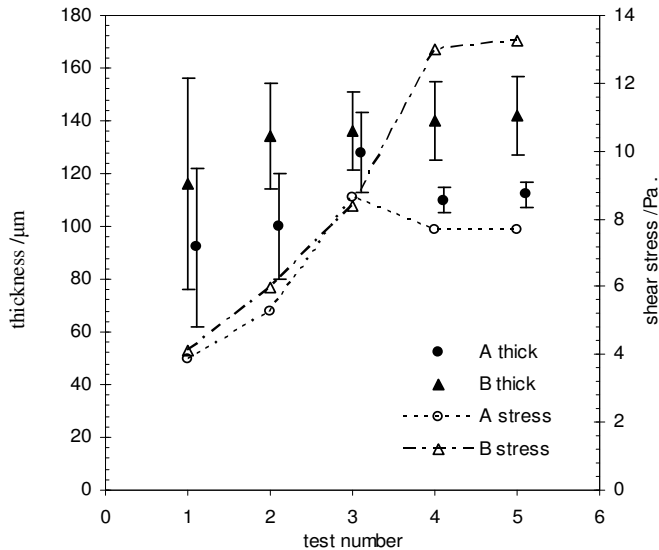


Figure 6 Successive measurements of thickness of *Synechococcus* biofilm grown on ss 304 substrate for 4 weeks. A and B refer to different locations on plate.

4.1 Apparatus

Biofilm testing was performed with a convergent nozzle similar to that in Figure 1 with dimensions $d_t = 2$ mm, $s = 0.5$ mm, $d = 4$ mm and internal nozzle angle of 45°. Both the tube and nozzle were constructed from 316 SS. A pressure tapping was located just above the divergent section and connected to a differential pressure transducer (Omega Engineering, PX26). A second tapping, located at the same elevation, was open to the reservoir and the difference in the transducer readings gave ΔP_{12} .

A computer-controlled syringe pump (Harvard Apparatus, PHD ultra, infuse only 703005) controlled the liquid flow. This device could only operate in expulsion mode, e.g. ejecting liquid rather than sucking, but this proved to work equally well. Flow rates used ranged from 0.4–1.0 g/s with an accuracy of 0.35%. The gauging liquid was water or salt solution at room temperature. In these experiments, the nozzle location was set manually: \dot{m} and ΔP_{12} were monitored by a PC running a Labview™ application, which automatically calculated the clearance and estimated wall shear stress at the nozzle throat. The calibration plot in Figure 7 shows that liquid ejection gave similar results to suction.

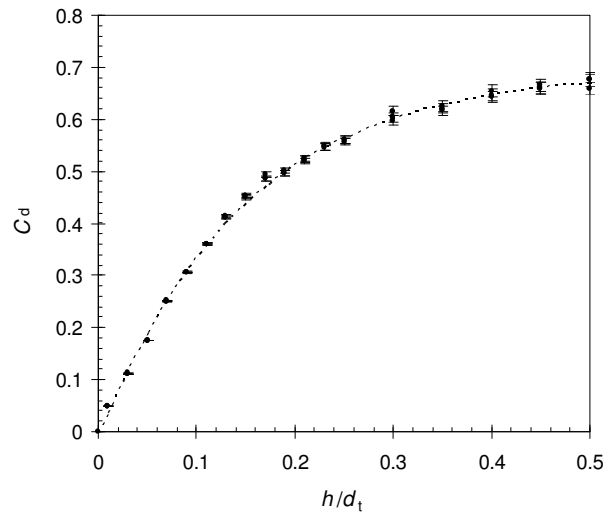


Figure 7 Calibration plot obtained with biofilm FDG nozzle, liquid ejection rate 0.6 g/s.

The sample was located on a base assembly which could be located on an optical or laser scanning confocal microscope so that the deposit layer could be imaged from beneath if the substrate was transparent (see Sahoo *et al.*, 2008). LED lights provided illumination for microscopy studies. The FDG nozzle was mounted on a frame which allowed the nozzle to be moved across a sample to make measurements at several locations. Further details of the apparatus are given in Salley *et al.* (2012).

4.2 Biofilms

Demonstration of pressure mode FDG for studying biofilms is provided in the form of a short investigation of the growth of the cyanobacterium *Synechococcus* sp. WH 5701. on three substrates, namely glass (microscope slide,

soda lime glass), 304 SS, and polyethylene terephthalate (PET) coated with a 1000 Å thick layer of indium tin oxide (ITO). The latter material is employed in photovoltaic applications as reported by Bombelli *et al.* (2011). Samples of the strain were obtained from the Culture Collection of Algae and Protozoa (CCAP; Oban, Scotland) and were prepared with assistance from Dr Alistair McCormick. A detailed description of the biofilm preparation protocol is given in Salley *et al.* (2012). Biofilms were grown under controlled lighting conditions over a period of four weeks. Samples were taken for analysis at the end of each week and subjected to thickness and (destructive) strength testing.

The electron micrograph in Figure 8 is representative of the well-developed biofilms, in that it shows a dense layer near the substrate and a looser, fluffy layer above. The two layers proved to have very different mechanical resistance. The shear stress required to deform the loose layer, labeled the deformation stress, varied from 5-30 Pa, while that required to deform the compact surface layer, labeled the rupture stress, was over 50 Pa on the steel and PET/ITO.

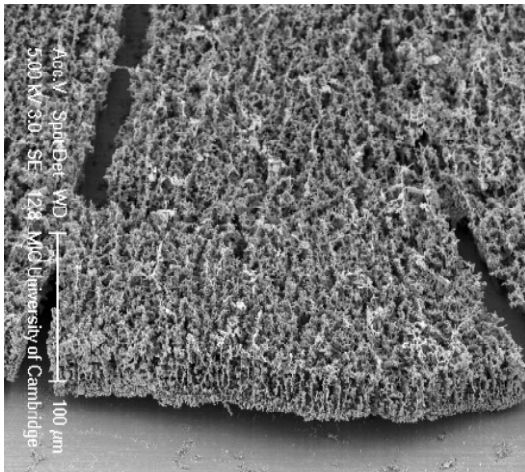


Figure 8 Scanning electron micrograph of *Synechococcus* biofilm grown on 304 SS for four weeks

Figure 9 is a summary of biofilm thickness measurements over the 4-week study. The cells formed layers whose thickness increased gradually with time from approximately 150 to 300 µm.

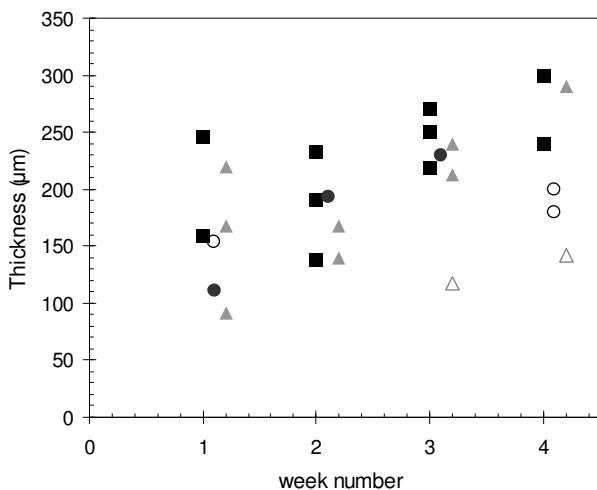


Figure 9 Average thickness of biofilms grown on stainless steel (triangles), PET/ITO (squares) and glass (circles). Three plates were tested each week. Empty symbols indicate biofilms where cell death was evident.

These layer thicknesses are comparable to those reported by other workers, albeit with different organisms (*e.g.* Mohle *et al.*, 2007) and represent an assembly of a few hundred cells stacked on top of each other. The variation in thickness between batches became smaller over time and indicated reproducible behaviour. The chlorophyll content of the biofilms increased steadily with time, indicating that the number of cells and density of the biofilms increased.

The adhesion behaviour of the biofilms differed markedly between glass and the other substrates. Figure 10(a) shows that the stresses imposed during thickness and strength measurement on PET/ITO was able to strip away the fluffy, upper biofilm layer. On glass, however, Figure 10(b) shows that the stresses were strong enough to disrupt the adhesive bonding to the substrate and cause rupture. Further results, as well as substrate characterization, are presented in Salley *et al.* (2012).

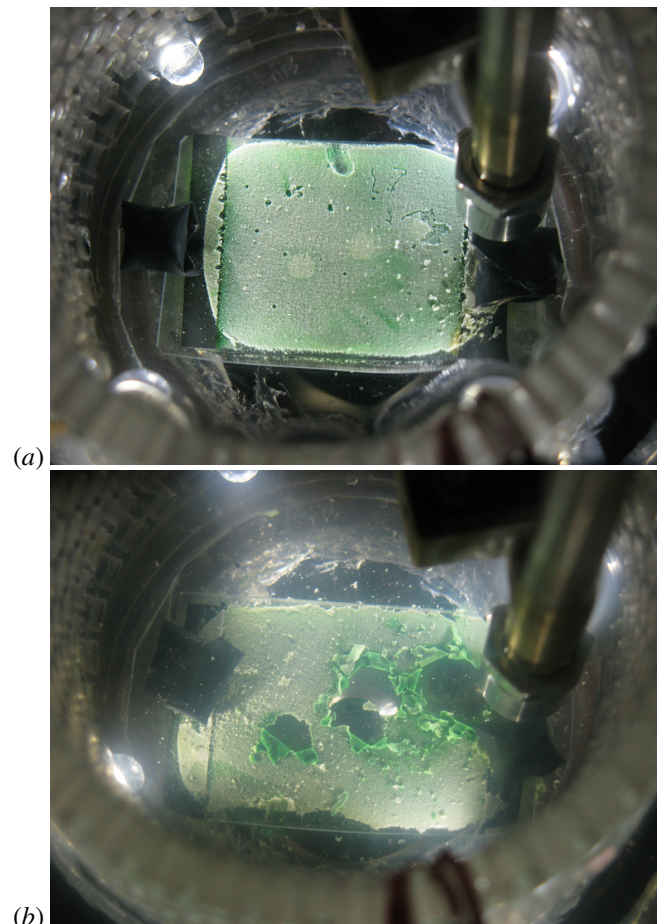


Figure 10 Photographs of 4 week old biofilms on (a) PET/ITO and (b) glass after thickness and strength measurement. Three locations were tested in each case. The rod on the right is the gauging nozzle.

CONCLUSIONS

1. Pressure mode FDG operation has been shown to offer several advantages, including (i) fixed gauging flow rate, (ii) insensitivity to operating pressure, and (iii) large pressure drops as the gauging nozzle approaches the surface which can be exploited for a proximity alarm.

2. The FDG device designed by Gu *et al.* (2009) for high pressure FDG has been commissioned and proof-of-concept results presented for oils at pressures up to 10 bara and temperatures up to 137°C. There is a lower working limit for the flow rate to yield a useful range of C_d values, given by $Re_t > 20$. CFD simulations of the flow patterns gave good agreement with the experimental observations.

3. Pressure mode FDG was used in low stress FDG measurements of the thickness of biofilms grown on three different surfaces. The thickness measurement accuracy has to be traded off against the shear stress imposed on the surface by the gauging flow. Biofilm thicknesses were determined to $\pm 10 \mu\text{m}$ and this proved sufficient to track the change of biofilm thickness over time. The cohesive and adhesive nature of the biofilms varied between substrates.

ACKNOWLEDGEMENTS

ESPRC DTA studentships for PWG and AA, supported by Procter & Gamble, are gratefully acknowledged, as is funding for BS from Ecole Polytechnique Palaiseau.

NOMENCLATURE

Latin

C_d	discharge coefficient	-
$C_{d\infty}$	discharge coefficient, asymptotic value	-
d	tube diameter	m
d_t	nozzle throat diameter	m
g	acceleration due to gravity	m/s ²
h	clearance	m
h_0	clearance between nozzle and substrate	m
\dot{m}	discharge mass flow rate	g/s
ΔP_{12}	pressure drop across nozzle	bar
P	absolute pressure	bara
Re_t	Reynolds number at nozzle throat	-
s	lip width	m
T	temperature	°C
v	velocity	m/s

Greek

δ	thickness of fouling layer	m
λ	nozzle entry length	m
μ	fluid viscosity	Pa s
ρ	fluid density	kg/m ³
φ	nozzle angle	-
τ	wall shear stress	Pa

REFERENCES

Ali, A., Chapman, G.J., Chew, Y.M.J., Gu, T., Paterson, W.R. and Wilson, D.I., 2013, A fluid dynamic

gauging device for measuring fouling deposit thickness in opaque liquids at elevated temperature and pressure, *Exptl. Thermal Fluid Sci.*, Vol. 48, pp 19-28

Bombelli, P., Bradley, *et al.*, 2011, Quantitative analysis of the factors limiting solar power transduction by *Synechocystis* sp PCC 6803 in biological photovoltaic devices, *Energy Env. Sci.*, Vol. 4 (11), pp. 4690-4698.

Chew, J.Y.M., Cardoso, S.S.S., Paterson, W.R. and Wilson, D.I., 2004a, CFD studies of dynamic gauging, *Chem. Eng. Sci.*, Vol. 59 (16), pp. 3381- 3398.

Chew, J.Y.M., Paterson, W.R. and Wilson, D.I., 2004b, Fluid dynamic gauging for measure the strength of soft deposits, *J. Food Eng.*, Vol. 65, 2, pp. 175 – 187.

Gordon, P.W., Brooker, A.D., Chew, Y.M.J., Wilson, D.I. and York, D.W., 2010, A scanning fluid dynamic gauging technique for probing surface layers, *Meas. Sci. Tech.*, Vol. 21, 085103.

Gu T., Albert F., Augustin W., Chew Y.M.J., Paterson W.R., Scholl S., Sheikh I., Wang K. and Wilson, D.I., 2011a, Fluid dynamic gauging applied to annular test apparatuses for fouling and cleaning, *Heat Transfer Eng.*, Vol. 32 (3-4), pp. 342-351.

Gu, T., Albert, F., Augustin, W., Chew, Y.M.J., Mayer, M., Paterson, W.R., Scholl, S., Sheikh, I., Wang, K. and Wilson, D.I. (2011b), Application of fluid dynamic gauging to annular test apparatuses for studying fouling and cleaning, *Exptl Thermal Fluid Sci.*, Vol. 35, pp. 509-520.

Gu, T., Chew, J.M.J., Paterson, W.R. and Wilson, D.I., 2009, Experimental and CFD studies of fluid dynamic gauging in annular flows, *AIChE J*, Vol. 55(8), pp. 1937-47.

Jones, S.A., Bird, M.R., Chew, Y.M.J. and Wilson, D.I., 2012, Fluid dynamic gauging of microfiltration membranes fouled with sugar beet molasses, *J. Food Eng.*, Vol. 108, pp. 22-29.

Lewis, W.J.T., Chew, Y.M.J., and Bird, M.R., 2012, The application of fluid dynamic gauging in characterising cake deposition during cross-flow microfiltration of a yeast suspension, *J. Membrane Sci.*, Vol. 405-406, pp. 113–122.

Lister, V.Y., Lucas, C., Gordon, P.W., Chew, J.Y.M., and Wilson, D.I., 2010. Pressure mode fluid dynamic gauging for studying cake build-up in cross-flow microfiltration, *J. Membrane Sci.*, Vol. 366, pp. 304-313.

Macchietto S., Hewitt G.F, *et al.*, 2010, Fouling in crude oil preheat trains: a systematic solution to an old problem, *Heat Transfer Eng.*, Vol. 32(3), pp. 197-215.

Middleman, S., 1998, *An Introduction to Fluid Dynamics: Principles of Analysis and Design*, Academic Press, New York, USA.

Mohle, R.B. Langemann, T. Haesner, M. Augustin, W., Scholl, S., Neu, T.R., Hempel, D.C. Horn, H., 2007, Structure and shear strength of microbial biofilms as determined with confocal laser scanning microscopy and fluid dynamic gauging using a novel rotating disc biofilm reactor, *Biotech Bioeng*, Vol. 98, pp 747 – 755.

Sahoo, P.K., Chew, J.Y.M., Mercadé-Prieto, R. and Wilson, D.I. (2008) Fluid dynamic gauging studies of swelling behaviour of whey protein in NaOH/NaCl solutions, *Intl. J. Food Sci. Tech.*, Vol. 43, pp 1901-1907.

Salley, B., Gordon, P.W., McCormick, A.J., Fisher, A.C. and Wilson, D.I. (2012), Characterising the structure

of photosynthetic biofilms using fluid dynamic gauging, *Biofouling*, Vol. 28(2), pp 159-173

Tuladhar, T.R., Paterson, W.R., Macleod, N. and Wilson, D.I., 2000, Development of a novel non-contact proximity gauge for thickness measurements of soft deposits and its application in fouling studies. *Can. J. Chem. Eng.*, Vol.78 (5), pp. 935 -947.

Tuladhar, T.R., Paterson, W.R. and Wilson, D.I., 2003, Dynamic gauging in duct flows. *Can. J. Chem. Eng.*, Vol. 81 (2). pp. 279-284.